Supplementary information for "Evaporation-driven ring and film deposition from colloidal droplets"

C. Nadir Kaplan[1] and L. Mahadevan[1,2,3,4]
[1] *School of Engineering and Applied Sciences, Harvard University, Cambridge, MA 02138, USA.*
[2] *Wyss Institute for Biologically Inspired Engineering, Harvard University, Boston, MA 02115, USA.*
[3] *Kavli Institute for Bionano Science and Technology, Harvard University, Cambridge, MA 02138, USA.*
[4] *Department of Physics, Harvard University, Cambridge, MA 02138, USA.*
(Dated: July 12, 2015)

A. Movies

1. Movie 1: The evolution of the liquid meniscus $h(r,t)$, solid height $h_s(r)$ and the local volume fraction $\Phi(r,t)$ of an evaporating droplet where $\Phi_0 = 5\times10^{-3}$ and $\eta = 2$.
2. Movie 2: The evolution of the liquid meniscus $h(r,t)$, solid height $h_s(r)$ and the local volume fraction $\Phi(r,t)$ of an evaporating droplet where $\Phi_0 = 0.05$ and $\eta = 2$.
3. Movie 3: The evolution of the liquid meniscus $h(r,t)$, solid height $h_s(r)$ and the local volume fraction $\Phi(r,t)$ of an evaporating droplet where $\Phi_0 = 0.12$ and $\eta = 2$.
4. Movie 4: The evolution of the liquid meniscus $h(r,t)$, solid height $h_s(r)$ and the local volume fraction $\Phi(r,t)$ of an evaporating droplet where $\Phi_0 = 0.05$ and $\eta = 5$.

B. Parameters and initial conditions used in section 4 in the main text

Using the physical parameters for the liquid-air interfacial tension $\gamma \sim 0.1$N/m, suspension density $\rho \sim 10^3$kg/m^3, gravitational acceleration $g \sim 10$m/s^2, bulk evaporation rate $E_0 \sim 10^{-6}$m/s, solvent viscosity $\mu \sim 10^{-3}$Pa·s, diffusion constant of the micron-sized colloidal spheres $D_s \sim 5\times10^{-11}$m^2/s, and the equilibrium contact angle $\theta_{e,0} = 15^o$, we find the capillary length $\ell_{cap} \sim 10^{-3}$m and the time scale $\tau = \tau(\eta,\theta_{e,0}) = \eta\epsilon\ell_{cap}/E_0 = \eta\epsilon 10^3$s. The dependence of the time scale on $\eta \equiv R^2/\ell_{cap}^2$ is shown in figure S5 in the supplementary data. Using these parameters, the capillary number is given as $Ca \equiv \mu E_0/\gamma = 10^{-8}$, and the Péclet number becomes $Pe^{-1} \equiv D_s/E_0R = 5\times10^{-2}$, so that $\alpha \gg 1$. We choose the scaled inverse pore size $\nu = 1$ since the effect of bigger ν on the formation of rings and bands is insignificant as long as $\alpha \gg \nu^2$ holds. This limit is discussed in section D below. The divergence of the evaporation rate at the contact line is resolved by assuming $E(r) = 1/\sqrt{1+\bar{\varepsilon}-r}$ when $r \to 1$, where $\bar{\varepsilon} = 0.01$.

The initial aspect ratio $\epsilon = \epsilon(\eta,\theta_{e,0})$ is specified by the hydrostatic height $h(r,0)$, demonstrated in figure S2(a) in the supplementary data. The initial particle distribution is given by $\Phi(r,0) = (\Phi_i - \Phi_0)e^{[r-L(0)]/d_0} + \Phi_0$, where $d_0 \ll 1$ and $L(0) = 1$.

C. Physical meaning of the closure between the solute and solvent velocities

In dimensionless units, the effective viscosity given by equation (2.5) in the main text becomes

$$\mu_{eff}(\Phi) = \frac{\mu\nu^3a^3h^3\Phi_c^\Gamma}{3\left(\nu ah - \tanh\nu ah\right)\left(\Phi_c^\Gamma - \Phi^{\Gamma+1}\right)}. \tag{S1}$$

We compare the Krieger-Doherty viscosity (red) and equation (S1) (black) in figure S1. We see that at low and intermediate Φ the two expressions agree very well. When $\Phi \sim \Phi_c$, equation (S1) yields a finite effective viscosity set by ν. The Krieger-Doherty relation diverges when $\Phi \to \Phi_c$, meaning that the fluid flow from the droplet interior into the deposit would vanish during drying.

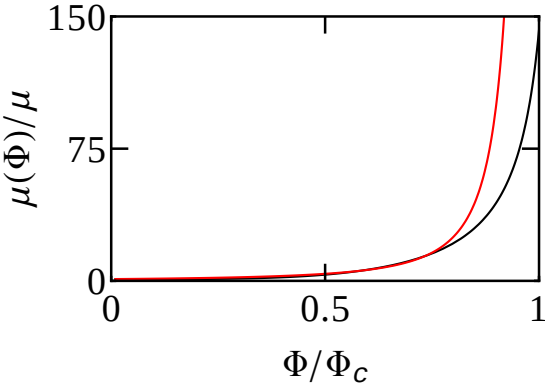

FIG. S1. The Krieger-Dougherty relation (red) and the effective viscosity relation from the Darcy-Brinkman equation (equation (S1), black) are demonstrated against the normalized volume fraction Φ/Φ_c. For the latter $\nu \equiv 10$ and $\Gamma = 4$.

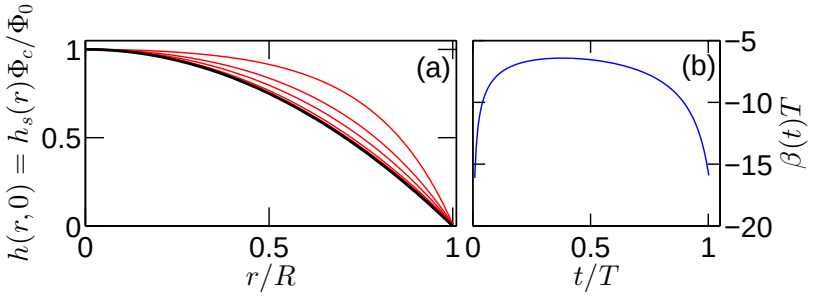

FIG. S2. Uniform film deposition ($\alpha \ll 1$, $Pe \gg 1$). (a) The relation between $h_s(r)$ and the initial hydrostatic profiles $h(r,0)$ as a function of increasing $\eta \equiv R^2/l_{cap}^2$, from bottom to top ($\theta_e = 15^o$). The black curve corresponds to the hydrostatic profile $h(r,t) = 1-r^2$ when $\eta \ll 1$. (a) is the solution to Eqs. (5) and (6) in the main text. Both $h_s(r)$ and $h(r,0)$ become more convex close to the contact line as η increases, corresponding to an approximate hydrostatically dominated pressure p (as schematically demonstrated in figure 1(d) in the main text). (b) The front propagation speed $\beta(t) = 1/\epsilon\partial_r t_c(r)$ collapses on a single curve with the corresponding scaling of the axes, where $T \equiv (\Phi_c - \Phi_0)/\Phi_c$ is the final deposition time of a uniform film (see the main text.

D. Effect of Marangoni flow on patterning

The Marangoni effect occurs when the surface tension at the liquid-air interface varies due to temperature or chemical gradients [1]. The variation of the surface tension induces a shear stress at the interface, driving the liquid toward regions of high surface tension. Here we assume that the chemical properties of the pure solvent are not altered

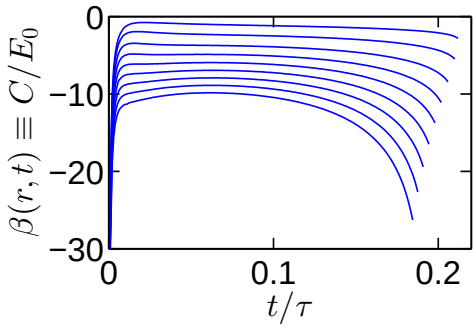

FIG. S3. Deposition rate of the rings or broad bands ($\alpha \gg 1$, $\eta = 1$). The deposition speed $\beta(t)$ as a function of increasing Φ_0 from top to bottom. The data correspond to $\Phi_0 \in \{5 \times 10^{-3} \cup [1.5 \times 10^{-2}, 0.12]\}$ in 1.5×10^{-2} increments. When Φ_0 increases, $\beta(t)$ decreases for all t and diverges faster at t_f.

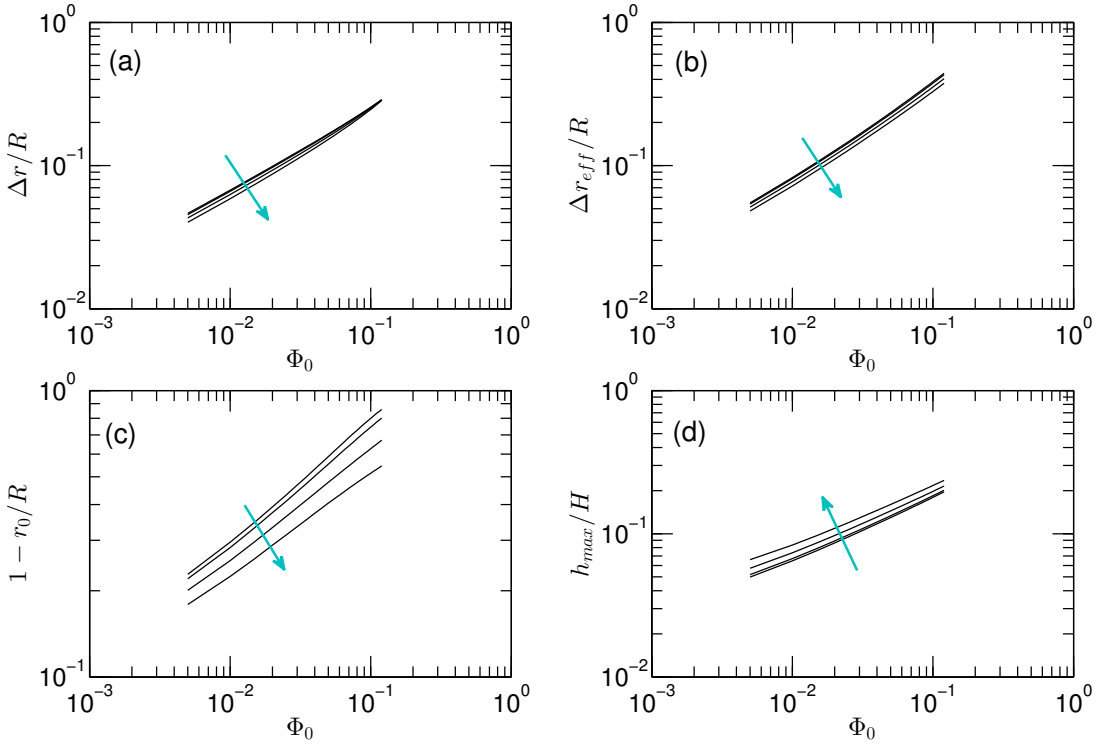

FIG. S4. Structural variables in the regime when $\alpha \equiv \epsilon^4/Ca \gg 1$, where $\epsilon = H/R$ is the aspect ratio of the drop, and $Ca = \mu E_0/\gamma$ is the Capillary number based on the evaporation rate E_0, the fluid viscosity μ and the surface tension γ. (a) the band width Δr, (b) the effective band width Δr_{eff}, (c) the dimensionless distance between the radius of the droplet and the meniscus touch-down location r_0, and (d) the maximum deposition height h_{max}, as a function of Φ_0 and $\eta \equiv R^2/\ell_{cap}^2$. Arrows denote the direction in which η increases, where $\eta \in \{0.1, 1, 2, 3\}$. Axes are given in the logarithmic scale.

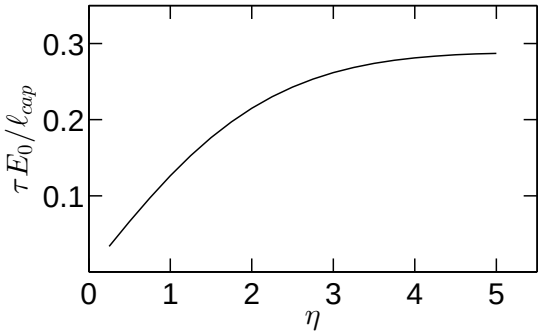

FIG. S5. The time scale $\tau = \tau(\eta, \theta_{e,0}) = \eta\epsilon\ell_{cap}/E_0$ of evaporation as a function of η at the ring formation ($\alpha \gg 1$).

due to colloids or other impurities, and hence only focus on the effect of temperature gradients. In the presence of a nonuniform surface tension profile, the viscous stress inside the liquid modifies to

$$\mu\partial v/\partial z = \partial p/\partial r(z-h) + \partial\gamma/\partial r\,. \tag{S2}$$

Following the discussion in section 1 of the main text and applying the chain rule $\partial\gamma/\partial r = \partial\gamma/\partial T \times \partial T/\partial r$, the scaling form of this expression is given as $\mu\alpha E_0/H\epsilon = \gamma H\epsilon/R^2 + \beta\Delta T_0/R$. Here $\beta \equiv \partial\gamma/\partial T$ is a property of the liquid ($\beta < 0$ in general) and $\Delta T_0 \equiv T_2 - T_1$ is the temperature difference between the contact line (T_2) and top of the droplet center (T_1). Then, the scaled inverse capillary number modifies to $\alpha_{Ma} = \alpha - \epsilon Ma$, where $Ma \equiv -\beta\Delta T_0\epsilon/E_0\mu$ is the Marangoni number. When $\Delta T_0 > 0$, then $Ma > 0$ and the Marangoni effect will suppress the ring formation as there arises a recirculating flow and α_{Ma} will become smaller or negative. This behaviour is particularly observed at sufficiently high contact angles and with solvents such as octane [2]. However, when $\Delta T_0 < 0$, then the ring formation will be reinforced since $\alpha_{Ma} > \alpha$. This especially occurs for low contact angles [3] and towards the end of drying. We

$\eta = 0.1$	$\alpha_{t,i}$	$\alpha_{t,f}$	$\sigma_{t,i}$	$\sigma_{t,f}$
$\Phi_0 = 5 \times 10^{-3}$	0.18	−0.03	−1.36	−0.10
$\Phi_0 = 0.05$	0.33	−0.02	−0.62	−0.05
$\Phi_0 = 0.12$	0.45	−0.04	−0.37	−0.1

TABLE S1. The scaling of Δr and β as a function of t initially, and in $t_f - t$ close to the meniscus touch-down, as extracted numerically for different volume fractions ($\eta = 0.1$). In dimensionless units, $\Delta r_i \sim t^{\alpha_{t,i}}$ is the initial ring width, $\Delta r_f \sim (t_f - t)^{\alpha_{t,f}}$ the final ring width, $\beta_i \sim t^{\sigma_{t,i}}$ the initial deposition rate, $\beta_f \sim (t_f - t)^{\sigma_{t,f}}$ the final deposition rate. The final time of meniscus touch-down is $t_f \sim 0.2H/E_0$.

	$\eta = 0.1$	$\eta = 1$	$\eta = 2$	$\eta = 3$
α	0.579	0.585	0.602	0.624
α_{eff}	0.668	0.666^*	0.66	0.657
β	0.429	0.417	0.387	0.357
χ	0.441	0.436	0.426	0.412

TABLE S2. The scaling of structural variables as a function of Φ_0 ($\eta \equiv R^2/\ell_{cap}^2$), as extracted from the slopes of the nearly linear profiles in figure S4 in logarithmic scale. In dimensionless units, $\Delta r \sim \Phi_0^{\alpha}$, $\Delta r_{eff} \sim \Phi_0^{\alpha_{eff}}$, $(1 - r_0) \sim \Phi_0^{\beta}$, $h_{max} \sim \Phi_0^{\chi}$.

have not taken the Marangoni effect into account in our analysis since it was found to be weak for water [2], which the material parameters in our analysis refers to.

E. Scaling of the ring width and deposition as a function of time ($\alpha \gg 1$)

When $\eta \ll 1$, the numerical scaling laws of the deposition speed β as well as the ring width Δr in early and late times for a range of volume fractions is given in Table S1.

F. Scaling of structural variables as a function of initial volume fraction ($\alpha \gg 1$)

In this section we will investigate the dependence of the structural variables on the initial colloidal volume fraction Φ_0 . These structural variables are; Δr (the ring width), Δr_{eff} (the effective ring width), the distance between the contact line and the touch-down location $1 - r_0/R$, and the maximum deposit height h_{max} . The effective ring width $\Delta r_{eff} \equiv \Delta r + \delta r$ accounts for the colloids in the left-over fluid tail, which are laid down after meniscus break-up. Thus, these particles also contribute to the width of the deposit at a length δr . We define δr in real units as

$$\delta r \equiv \frac{1}{R\bar{h}} \int_{r_0}^{r_i} r dr \Phi(r) h(r) \,, \tag{S3}$$

where

$$\bar{h} \equiv \frac{1}{R(r_i - r_0)} \int_{r_0}^{r_i} r dr h(r) \,, \tag{S4}$$

and $r_i = r_i(t_f)$ is the final position of the deposition front at the meniscus touch-down (see main text). The contact line radius is taken to be unity ($R = 1$) in dimensionless units.

The scaling exponents are given in Table II as a function of $\eta = R^2/\ell_{cap}^2$. At $\eta = 1$, $\alpha_{eff} = 0.666$ (denoted by *) agrees well with experiments [4].

[1] de Gennes, P. G. 1985 Wetting: statics and dynamics. *Rev. Mod. Phys.* **57**, 827–863.
[2] Hu, H. & Larson, R. G. 2006 Marangoni effect reverses coffee-ring depositions *J. Phys. Chem. B.* **110**, 7090–7094.
[3] Hu, H. & Larson, R. G. 2005 Analysis of the effects of Marangoni stresses on the microflow in an evaporating sessile droplet *Langmuir* **21**, 3972–3980.
[4] Deegan, R. D. 2000 Pattern formation in drying drops. *Phys. Rev. E: Stat., Nonlinear, Soft Matter Phys.* **61**, 475–485.